Published on 15 May 2023. Downloaded by Ecole Sup de Physique et de Chimie Industrie on 5/22/2023 10:56:37 AM.

Soft Matter

PAPER

View Article Online
View Journal

Check for updates

Cite this: DOI: 10.1039/d3sm00194f

Computational design of a minimal catalyst using colloidal particles with programmable interactions†

Maitane Muñoz-Basagoiti, [a] Olivier Rivoire*[ab] and Zorana Zeravcic *[a]

Received 14th February 2023,
Accepted 13th May 2023

DOI: 10.1039/d3sm00194f

rsc.li/soft-matter-journal

Catalysis, the acceleration of chemical reactions by molecules that are not consumed in the process, is essential to living organisms but remains absent in physical systems that aspire to emulate biological functionalities with artificial components. Here we demonstrate how to design a catalyst using spherical building blocks interacting *via* programmable potentials, and show that a minimal catalyst design, a rigid dimer, can accelerate a ubiquitous elementary reaction, the cleaving of a bond. Combining coarse-grained molecular dynamics simulations and theory, and by comparing the mean reaction time for bond dissociation in the presence and absence of the catalyst, we derive geometrical and physical constraints for its design and determine the reaction conditions under which catalysis emerges in the system. The framework and design rules that we introduce are general and can be applied to experimental systems on a wide range of scales, from micron size DNA-coated colloids to magnetic handshake materials in the macroscale, opening the door to the realization of self-regulated artificial systems with bio-inspired functionalities.

1 Introduction

Bio-inspired design combines principles from physics, chemistry, biology and engineering to create artificial materials with functionalities that rival those of biological systems, paving the way for the next generation of "smart" materials. One of the key ingredients for biological self-assembly and self-organization is the specificity of interactions between building blocks at the molecular scale. This has motivated an enormous experimental progress over the last decades in making artificial building blocks that differ in shape, size and types of interactions. For example, single stranded DNAs grafted on the surface of nano- and micron size particles lead to short-range binding specificity which controls what particle types can interact,[1–6] patchy and asymmetric particles can be used for directional bonding with valence control,[7,8] and mobile DNA linkers on colloidal particles and emulsion droplets lead to valence control without predetermined particle geometry.[9–12] Following these advances, model systems based on such artificial building blocks have been used in experiments, theory and simulations to demonstrate desired bio-inspired properties like robust and reliable self-assembly into target structures,[4,13–22] structure reconfiguration[23–25] and self-replication.[26–29]

A major obstacle for efficiency and scalability in these artificial systems is the control over the formation and cleavage of targeted bonds. For instance, escaping kinetic traps, which are detrimental for the self-assembly yield of target structures,[22,30–32] requires breaking bonds between particular building blocks. Likewise, in artificial self-replicating systems bonds between specific building blocks must successively form and break in a timely manner.[27,28,33] The efficiency of these and many similar processes currently relies on external intervention such as temperature and UV cycling protocols or mechanical forcing, which can non-specifically impact all the bonds in the system.[26,28,33,34] Nature, however, does it differently. In biological systems, reactions are facilitated by catalysts – enzymes – which, besides being extremely efficient and specific, are not energy consuming and are systematically recycled. Realizing this level of control with designed building blocks will open the way for self-regulation in artificial systems that aim to emulate living matter. One of the major challenges to reach this goal is therefore to build tailor-made catalysts out of artificial building blocks.

Over many decades, several qualitative principles for catalysis design have been formulated, including notably Haldane's principle of strain-based catalysis,[35] Pauling's principle of complementarity to the transition state[36] and Sabatier's principle of "just-right" interaction strength.[37] These principles address different aspects of the design of a catalyst, but they do not constitute a general framework to build artificial catalysts from

[a] Gulliver UMR CNRS 7083, ESPCI Paris, Université PSL, 75005 Paris, France. E-mail: olivier.rivoire@espci.fr, zorana.zeravcic@espci.fr
[b] Center for Interdisciplinary Research in Biology (CIRB), Collège de France, CNRS, INSERM, Université PSL, 75005 Paris, France

† Electronic supplementary information (ESI) available. See DOI: https://doi.org/10.1039/d3sm00194f

Published on 15 May 2023. Downloaded by Ecole Sup de Physique et de Chimie Industrie on 5/22/2023 10:56:37 AM.

scratch for any desired reaction. As a result, successful designs of physical catalysts have so far relied on astute mechanisms that are not readily applicable beyond their original context,[38–40] and only recently general considerations for catalysis have been investigated in an abstract model, shedding light on the constraints that apply to the design of a catalyst.[41] There is thus a need for empirical and theoretical insights with a bottom-up approach that integrates kinetic, geometrical and physical constraints to enable the design of catalysts that are experimentally implementable in physical systems.

To make the first steps towards this goal, here we present the computational design of a minimal catalyst capable of accelerating the dissociation of a dimer into monomers, *i.e.*, cleaving a bond. Starting from building blocks interacting *via* programmable potentials, we provide rules for making a catalyst and test our design in numerical simulations of a physical model system. The framework and design rules we introduce can be applied to experimental systems spanning different length scales, from nanoparticles and micron size DNA-coated colloids[4] to centimeter size magnetic handshake materials.[42]

2 Model system

2.1 Spontaneous reaction

The design of a catalyst depends on the reaction it accelerates. Here we focus on the dissociation of a dimer S = M·M into two free monomers P = M + M, which we refer to as the substrate S and the product P of the reaction (Fig. 1(A)). The substrate dimer is composed of two spherical particles of diameter σ interacting *via* an isotropic pairwise potential of depth ϵ_s and interaction range r_{cutoff}[43] (see ESI†), which, if exceeded, leads to the dissociation of the dimer into monomers (Fig. 1(B)). Inspired by the short-range interactions between colloids mediated by DNA (through direct hybridization or by using linkers),[4,44] we set the interaction cutoff to be $r_{cutoff} = 1.10\ \sigma$, which results in $r_{min} = 1.03\ \sigma$ as the equilibrium position of the substrate bond. We consider two limiting cases for the reaction between the free monomers: the irreversible limit case, when the reformation of the bond between monomers is forbidden (ESI†) and the case when bond formation is diffusion-limited, see Fig. 1(B). In what follows, we take $k_BT = 1$ for the energy scale and $\sigma = 1$ for the length scale in our system. The transition from the dimer to the two-monomer state occurs spontaneously through thermal activation. We perform Molecular Dynamics (MD) simulations of this system (see ESI†) and verify that the dissociation events, defined as the first time the distance between two monomers exceeds $r > r_{cutoff}$, are exponentially distributed with mean reaction time $T_{S\to P}$ (ESI,† Fig. S1), where we use the subindex S → P to denote the transformation of one substrate dimer to one product (two monomers). The mean time $T_{S\to P}$ is the key parameter that we will use for the assessment of catalysis.

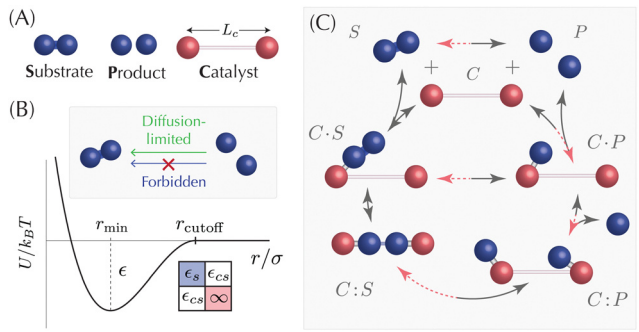

Fig. 1 Simulation model parameters. (A) Our system consists of a substrate dimer *S* that can dissociate into two free product monomers *P* (in blue), and a catalyst *C* (in red). The particles in the catalyst are kept at a fixed distance L_c. (B) We use a short-range pairwise interaction potential with depth ϵ, interaction range r_{cutoff} and equilibrium position r_{min}.[43] As indicated by the interaction matrix, blue particles interact with strength ϵ_s, and blue and red particles interact with strength ϵ_{cs}; the catalyst bond is rigid. The association of two substrate monomers (grey box) can be diffusion-limited or forbidden (irreversible reaction). (C) Reaction scheme in the presence of the catalyst. Gray arrows correspond to the most favourable reaction conditions for catalysis: free monomers are removed from the system and the substrate bond is not allowed to reform once broken by the catalyst; dashed red arrows correspond to the worst-case conditions, where the above transitions are reversible and diffusion-limited.

2.2 Catalyst design

To build a minimal catalyst we use the same-sized spherical particles that comprise the substrate. As we verify in numerical simulations, a single particle cannot catalyze the dissociation reaction (ESI,† Fig. S2). The next simplest design is a dimer made of two particles whose centers are held at a distance L_c. Motivated by previous theoretical results,[41] we set the catalyst bond to be rigid (ESI†). Each catalyst particle can interact with a substrate particle *via* the potential in Fig. 1(B),[43] with a strength ϵ_{cs} and an interaction range that we constrain to be the same r_{cutoff}. Bond formation between catalyst and substrate particles is diffusion-limited. For simplicity, we assume that particles exhibit valence: a catalyst particle can interact with only one substrate particle at a time, while a substrate particle can interact with only one substrate and only one catalyst particle at the same time. This type of restricted binding has been achieved in experiments with colloidal particles,[11,45,46] while the fixed distance L_c between catalyst particles could be realized experimentally by placing them on a surface.

2.3 System parameters

Catalysis depends on three sets of parameters. First, it depends on the reaction to be accelerated, characterized by the overall shape of the interaction potential, and the entropic barriers for the forward and the reverse direction. In our simple model, these are controlled by the strength of the bond we want to cleave, ϵ_s, and by the (ir)reversibility of the spontaneous reaction respectively. These parameters span a family of spontaneous reactions that we aim to accelerate. Second, catalysis depends on the intrinsic properties of the catalyst, like its geometry and types of interactions. These correspond to the two particles rigidly bound, placed at a fixed distance L_c and the interaction strength towards the substrate ϵ_{cs} in our model. Finally, catalysis depends on extrinsic properties of the system such as the

This journal is © The Royal Society of Chemistry 2023

Published on 15 May 2023. Downloaded by Ecole Sup de Physique et de Chimie Industrie on 5/22/2023 10:56:37 AM.

concentration of substrate and product and their diffusion constant, as well as the volume and temperature of the system, which we will discuss in more detail elsewhere.[47]

Our goal here is to identify intrinsic parameters of the catalyst that lead to catalysis in the system. To assess if there is catalysis, we consider a box of volume V with a single substrate, and compare the mean reaction time in the absence and presence of a single catalyst in the system, *i.e.*, compare the mean first-passage times $T_{S\to P}$ to $T_{C+S\to C+P}$, where C + S and C + P account for the substrate and product particles in the presence of, but not interacting with the catalyst. A successful catalytic design must reduce the mean reaction time, and our criterion for catalysis is $T_{S\to P}/T_{C+S\to C+P} > 1$. To proceed, we first explore the parameter space under two assumptions that are most favorable for catalysis, and then investigate what happens when we lift them. The first assumption is that the spontaneous reaction is irreversible, preventing the spontaneous formation of substrate bonds once broken. The second assumption is that the product monomers are removed from the system as soon as they are released in solution—through either spontaneous unbinding from the catalyst or the spontaneous reaction happening while bound to the catalyst—therefore preventing them from (re)binding any other particle in the system. In the setup shown in Fig. 1(C), red arrows correspond to the four backward processes that are excluded due to these assumptions.

3 Results

3.1 Conditions for catalysis

In order to identify necessary conditions for catalysis, we decompose the catalytic cycle into elementary processes, each of which corresponds to the formation or cleavage of a single bond. As illustrated in Fig. 1(C), this defines six possible states of the system: C + S, where the substrate and catalyst are not interacting; C·S, where the substrate forms one bond with the catalyst; C:S, where both substrate particles are bound to the catalyst; C:P, where the substrate bond has been cleaved and both products remain bound; C·P, where one product particle has been released into the solution and the second one remains bound; and finally C + P, where the two product particles are released by the catalyst, which recovers its initial state. The reaction C·S → C·P corresponds to the spontaneous dissociation of the substrate bond while the substrate is partially bound to the catalyst. The series of reactions from state C:S up until the recycling of the catalyst in C + P comprise an alternate pathway to reach the final product state exclusively due to the presence of the catalyst.

A trivial necessary condition for catalysis is that the state C:S is accessible from C·S. Otherwise, the only way for product particles to appear in solution is through the transitions S → P and C·S → C·P, *i.e.*, through the spontaneous reaction. This condition constrains the distance between the catalyst particles L_c to be small enough and imposes favorable binding between the catalyst and the substrate, *i.e.*, $L_c < 3r_{cutoff}$ and $\epsilon_{cs} > 0$, respectively.

Next, one expects the transition from C:S to C + P to take on average less time than the spontaneous reaction S → P, *i.e.*, the product must be formed faster through the interaction with the catalyst than spontaneously. This implies necessary conditions on the elementary steps (i) C:S → C:P, (ii) C:P → C·P and (iii) C·P → C + P. Process (i) must satisfy the necessary condition $T_{C:S\to C:P\backslash C\cdot S} < T_{S\to P}$, where $T_{C:S\to C:P\backslash C\cdot S}$ denotes the mean first-passage time from C:S to C:P excluding the possibility of the back transition to the state C·S. In other words, cleaving the substrate bond in the presence of the catalyst should be faster than in its absence. To find which parameters this condition constrains, we perform MD simulations of one catalyst and one substrate in a box initiated in C:S configuration, with fixed ϵ_s, and $\epsilon_{cs} \gg 1$ to avoid substrate unbinding (ESI,† Fig. S2). By varying the geometry of the catalyst we find that the condition can be satisfied only if $L_c > 3r_{min}$. At $L_c = 3r_{min}$, which corresponds to the geometrical threshold above which the substrate can fit between the particles in the catalyst, the C:S configuration is one-dimensional (see Fig. 1(C)) and all the bonds are in equilibrium. For larger L_c, the bonds are stressed, leading to the substrate bond being strained by the catalyst.

Steps (ii) and (iii), namely, breaking the two ϵ_{cs} bonds with the catalyst, lead to the additional necessary conditions $T_{C:P\to C\cdot P\backslash C:S} < T_{S\to P}$ and $T_{C\cdot P\to C+P\backslash C:P} < T_{S\to P}$. Given that these two steps correspond to the same process, and that the catalyst releases product monomers independently, both conditions are satisfied if $T_{C\cdot P\to C+P\backslash C:P} < T_{S\to P}$. Simply, releasing one product particle should be faster than the spontaneous reaction. This condition depends only on how strongly the product is bound to the catalyst, and is satisfied by imposing $\epsilon_{cs} < \epsilon_s$, *i.e.*, the interaction between S and C should be weaker than the scissile bond in the substrate (see ESI†).

No similar conditions apply to the remaining two elementary steps towards C + P in Fig. 1(C), namely, transitions C + S → C·S and C·S → C:S. First, the emergence of catalysis is independent of the time it takes the substrate to find the catalyst $T_{C+S\to C\cdot S}$, because the spontaneous dissociation of the substrate into two monomers can always occur along the way. Second, the necessary condition on $T_{C\cdot S\to C:S}$ non-trivially involves mean reaction times of other elementary steps in the catalytic pathway because of the $C{\cdot}S \to C{\cdot}P$ transition. As a result, no simple additional constraint on the catalyst design can be derived. We discuss these transitions in more details in the ESI† and more formally in.[47]

3.2 Phase diagram for catalysis

For a given spontaneous reaction, *i.e.*, for a given ϵ_s in the irreversible limit, and based on the above analysis, the necessary conditions for catalysis in our model constrain the design parameters for the dimer catalyst to $3r_{min} < L_c < 3r_{cutoff}$ and $0 < \epsilon_{cs} < \epsilon_s$. We perform MD simulations of the system within this parameter range starting from a single substrate dimer and with or without a single catalyst present, and compare the mean reaction times to produce two free monomers in both cases. Our results for a 2-dimensional (2D) system are shown in the phase diagrams in Fig. 2.

Published on 15 May 2023. Downloaded by Ecole Sup de Physique et de Chimie Industrie on 5/22/2023 10:56:37 AM.

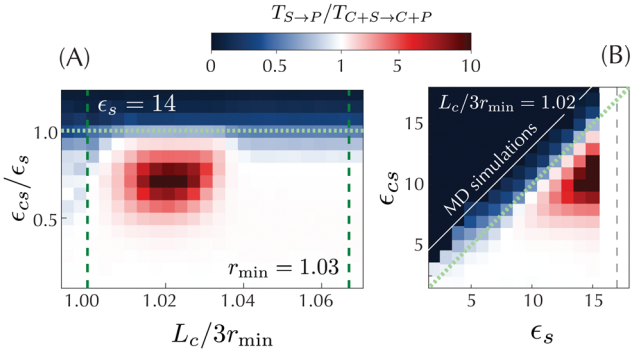

Fig. 2 Phase diagram of catalysis. Simulation results for a 2D system under conditions that are most favorable for catalysis, *i.e.*, systematic product removal and irreversible spontaneous reaction. The simulation box length is $L = 7.5$. Event statistics over which the average reaction times are computed are shown in ESI,† Fig. S3. (A) For a fixed spontaneous reaction ($\epsilon_s = 14$) in the irreversible limit, catalysis, *i.e.*, $T_{S\to P}/T_{C+S\to C+P} > 1$, requires $3r_{\min} < L_c < 3r_{\text{cutoff}}$ (green dashed lines) and $\epsilon_{cs}/\epsilon_s < 1$ (green dotted line). Catalysis (in red) is indeed observed only within these bounds. (B) Fixing the catalyst geometry ($L_c/3r_{\min} = 1.02$) shows that there is a minimal ϵ_s required for catalysis. The diagonal green dotted line represents the $\epsilon_{cs}/\epsilon_s < 1$ constraint. The white solid line separates simulated data (below) from extrapolated data (above). The grey dashed line gives an indication of experimental time of 1 s for a model system of colloids with $\sigma = 1$ μm at room temperature.

In Fig. 2(A) we show catalytic efficiency for different values of L_c and ϵ_{cs}, keeping ϵ_s fixed, where we demonstrate that catalysis can occur within the range of identified necessary conditions (dashed and dotted lines). The maximum in the heat map reveals the best design for the catalyst for the chosen $r_{\text{cutoff}} = 1.1\sigma$ (ESI†). In Fig. 2(B) we now fix the catalyst geometry L_c and vary ϵ_s and ϵ_{cs}, showing again that catalysis occurs within the range of necessary conditions. Our detailed simulations in the prescribed (ϵ_{cs},L_c,ϵ_s) parameter space reveal that catalysis requires a minimal value of ϵ_s (Fig. 2(B)). This is another condition on catalysis that applies to the spontaneous reaction rather than to the catalyst design itself. We interpret this result through two arguments. Firstly, if the spontaneous reaction occurs too fast, the substrate will dissociate before it can bind the catalyst in the right configuration. Secondly, the catalyst inhibits the reaction for too small ϵ_s because the substrate is able to diffuse to the catalyst, reaching the C·S state, but the bond breaks at its spontaneous rate along the C·S → C·P pathway instead of using the catalytic mechanism. One of the monomers is released in solution, while the second one remains attached on the surface of the catalyst. Since the reaction ends only once there are two free monomers in solution, and the catalytic pathway contains the extra step of release which does not exist for the spontaneous reaction, the design effectively inhibits the reaction by delaying the production of free monomers. As energies are here given in units of k_BT, this last condition indicates a threshold temperature above which catalysis does not occur anymore.

3.3 Trade-offs

Our phase diagram in Fig. 2 reveals trade-offs applying to the geometry L_c of the catalyst and how strongly it binds the substrate ϵ_{cs}. These trade-offs emerge from considering all elementary steps in the catalytic cycle simultaneously.

In the case of the catalyst geometry, within the bounds $3r_{\min} < L_c < 3r_{\text{cutoff}}$, there is an optimum L_c that maximizes the strain on the substrate bond while minimizing the time to fully bind the substrate. The strain is greater the more complementary the catalyst is to the transition state (ESI,† Fig. S2), in agreement with Pauling's principle,[48] where exact complementarity in our model implies $L_c/3r_{\min} = 2/3 + r_{\text{cutoff}}/3r_{\min} = 1.023$ (see ESI†). However, adopting this configuration takes long time (ESI,† Fig. S4), giving rise to the trade-off.[49] In the case of the catalyst–substrate bond, the optimal strength ϵ_{cs} maximizes the strain on the substrate while minimizing the time to release the product particles into solution, which embodies Sabatier's principle[37] of optimal intermediate binding strength.

3.4 Coarse-graining and relaxing constraints

To examine the conditions for catalysis beyond the restrictive assumptions that we made so far – irreversible reaction and systematic removal of products – we follow the approach usually taken in chemistry to coarse-grain chemical reactions as Markov processes.[50] Under this approximation, a larger range of parameters can be more efficiently explored. In general, one cannot assume that all the steps in a cycle (as in Fig. 1(C)) can be represented as Markov transitions. We verify, however, that this is the case in our model system within the range of parameters necessary for catalysis, which means that the rates for the transition between states can be inferred from our simulations, an approach previously applied in other MD studies[51–53] (ESI,† Fig. S5). We use rates inferred from MD simulations to verify the coarse-graining (see ESI†), and the resulting Markov State Model (MSM) is shown in Fig. 3(A). To extend the exploration of the parameter space, we develop an analytical model for the dependency of the rates on the parameters (see ESI†) that we use in all MSM calculations that follow.

We first consider relaxing only the condition that the reaction is irreversible. In the MSM we therefore introduce a parameter $\gamma \in [0,1]$ as a prefactor to the rates corresponding to diffusion-limited transitions C·P → C·S and C:P → C:S. This allows us to interpolate and consider families of spontaneous reactions that lie between the diffusion-limited cases ($\gamma = 1$) and the irreversible ($\gamma = 0$) limit of substrate bond formation (Fig. 3(A)). In Fig. 3(B) we show maximal catalytic efficiency for increasing substrate bond strength ϵ_s at different values of the parameter γ (black lines). For $\gamma = 0$, the maximal efficiency of our catalyst scales exponentially with ϵ_s. When $\gamma > 0$, the transition C:P → C:S is possible. As a result, an additional constraint on catalysis arises, which couples the cleavage of the substrate bond and release of the first product monomer to the reformation of the substrate bond. This condition is responsible for the saturation of the catalytic efficiency at high ϵ_s seen in Fig. 3(B). These Markov state model results agree with our MD simulations in the irreversible limit and diffusion-limited case, shown as blue triangles and green circles in the figure,

 This journal is © The Royal Society of Chemistry 2023

Published on 15 May 2023. Downloaded by Ecole Sup de Physique et de Chimie Industrie on 5/22/2023 10:56:37 AM.

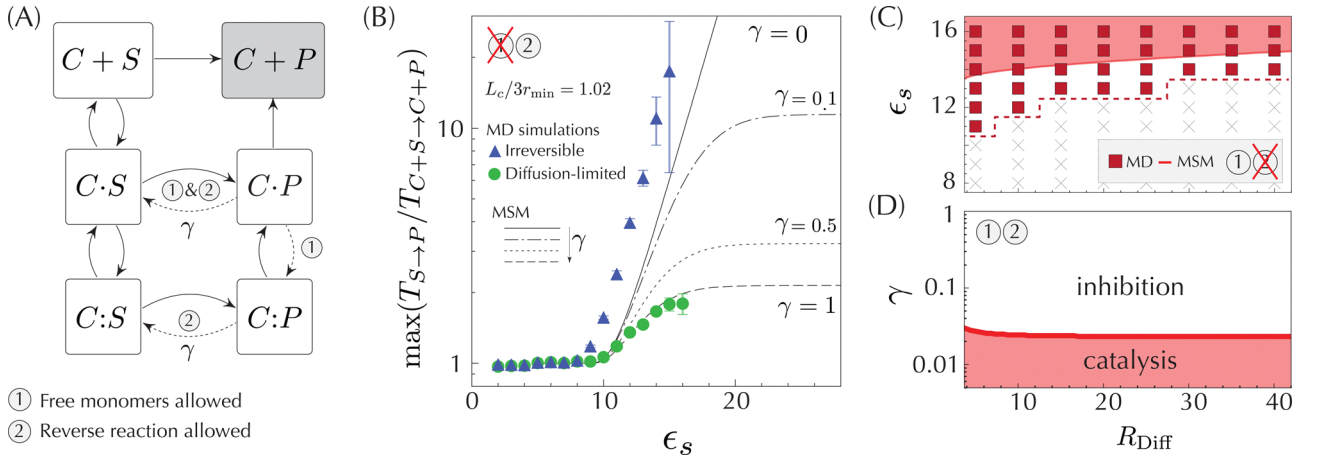

Fig. 3 Lifting assumptions in the model. (A) Structure of the Markov State Model (MSM) inferred from MD simulations showing the states of the system in the presence of the catalyst. The reaction is over when state C + P, colored in gray, is reached. We consider two different assumptions on the model: (1) removing monomers as soon as they are released into solution; and (2) limiting the reformation of the substrate bond through the parameter $\gamma \in [0,1]$, with $\gamma = 1$ corresponding to diffusion-limited reactions and $\gamma = 0$ to irreversible ones. Dashed arrows indicate the transitions affected by these constraints. (B) Maximal catalyst efficiency, $\max(T_{S\to P}/T_{C+S\to C+P})$, when free monomers are removed from the system as a function of the substrate bond strength ϵ_s for a fixed geometry of the catalyst $L_c/3r_{min} = 1.02$. Data points correspond to 2D MD simulations and black lines to the MSM depicted in panel A. The maximal efficiency in the model, which is obtained when $\gamma = 0$, scales exponentially as $\propto e^{\alpha\epsilon_s}$, with a factor $\alpha_{MD} = 0.50 \pm 0.04$ (the fit is conducted for points where the efficiency is larger than one, *i.e.*, $\epsilon_s \geq 8$) and $\alpha_{MSM} = 0.44$. The maximal efficiency saturates for large ϵ_s when $\gamma \neq 0$. (C) Substrate bonds ϵ_s for which catalysis is observed (red) in a 2D system with free monomers removed only after they have diffused a distance R_{Diff} from the catalyst. We keep the spontaneous reaction irreversible, *i.e.*, $\gamma = 0$. Red region represents results from the Markov model and red squares are results from our MD simulations. White region and gray crosses mark the regions where catalysis is not possible in the model and simulations respectively. (D) MSM results showing the γ values for which catalysis can be observed in 2D when monomers are removed from the system if they have diffused a distance R_{Diff} from the catalyst.

validating the coarse-graining of the catalytic pathway into states (see ESI† for additional validations).

Next we explore whether we can measure catalytic activity of our dimer catalyst if free monomers are not taken out of the system as soon as they are released into the solution. To do this, we introduce a disk of radius R_{Diff} centered around the catalyst and consider that we have reached the C + P state only once both free monomers diffuse out of this volume (ESI,† Fig. S7). Results we obtain from the MSM when $\gamma = 0$ are shown in Fig. 3(C) (red shaded region). As can be seen, under these conditions, the onset of catalysis depends on the volume of the disk around the catalyst: the larger the volume, the longer it takes free monomers to diffuse out, which implies that the spontaneous reaction must be slower, *i.e.*, the minimal ϵ_s should be larger to observe catalysis in our model. Our 2D MD simulations, reporting the minimal substrate bond strength at which we observe catalysis in the irreversible limit (red squares), agree with the Markov model predictions.

Finally, when $\gamma > 0$, our MSM predicts catalysis in 2D to be possible only for a range of $\gamma < \gamma_{max}$ values, as shown in Fig. 3(D). In other words, our model predicts that beyond the most favorable conditions, the reverse reaction cannot be diffusion-limited, and that some finite barrier is necessary in order to observe catalysis. To verify this prediction in MD simulations requires first changing how particles interact, *i.e.*, introducing a finite backward reaction barrier, and second expanding the range of substrate bond strengths explored, which becomes computationally more challenging as ϵ_s grows. We leave this verification for future work. Results for a 3D system are shown in the ESI.†

3.5 Efficiency and optimality of the catalyst design

Motivated by possible experiments to be discussed below, we quantify the efficiency of our catalyst as function of bond strengths in the conditions where the product is not immediately removed, while the catalyst geometry (L_c) is kept fixed and the spontaneous reaction is irreversible. We first focus on the effect R_{Diff} (volume) has on the maximal efficiency, which is represented by blue triangles in Fig. 3(B). While our simulation results in Fig. 4(A) show (as expected) that the maximal efficiency decreases with increasing volume (increasing R_{Diff}), our minimal catalyst for a given spontaneous reaction (fixed ϵ_s) still succeeds in accelerating the spontaneous reaction several fold and the maximal efficiency still scales exponentially in the limit $\epsilon_s \gg 1$ (ESI,† Fig. S8). Moreover, our simulations demonstrate the robustness of our catalyst design. First, as seen in Fig. 4(A), the optimum $\epsilon_{cs}/\epsilon_s \approx 0.6$ remains unchanged as the volume varies. Second, as seen in Fig. 4(B), the optimum ϵ_{cs}/ϵ_s remains unchanged also when ϵ_s varies for fixed R_{Diff}. In other words, the curves of catalytic efficiency, known as Volcano plots in the catalysis literature,[54,55] share approximately the same optimum ϵ_{cs}/ϵ_s.

4 Discussion

We have taken a first step toward introducing catalysis in a system of colloidal particles by presenting design rules for constructing the simplest possible catalyst – a rigid dimer – that can accelerate bond dissociation. Our design is directly

Published on 15 May 2023. Downloaded by Ecole Sup de Physique et de Chimie Industrie on 5/22/2023 10:56:37 AM.

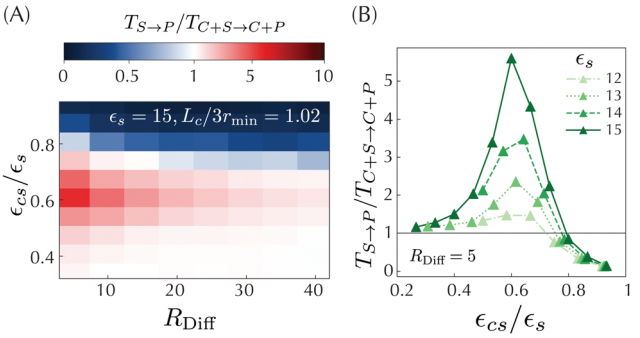

Fig. 4 Efficiency and catalyst design beyond most favourable reaction conditions. MD simulation results in 2D when free monomers are removed if they diffuse beyond $r > R_{\mathrm{Diff}}$, where R_{Diff} is the radius of a disk centered around the catalyst (Fig. S7, ESI†). The spontaneous reaction is assumed to be irreversible. (A) Catalytic efficiency, $T_{S\to P}/T_{C+S\to C+P}$ for a fixed substrate bond with $\epsilon_s = 15$ and catalyst geometry $L_c/3r_{\min} = 1.02$, for different simulation box sizes and varying ϵ_{cs}. (B) Volcano plots showing the optimal catalyst binding strength ϵ_{cs} for a fixed volume $R_{\mathrm{Diff}} = 5$ and varying substrate bonds. The optimal ϵ_{cs}/ϵ_s remains unchanged as ϵ_s varies. The average for each data point is taken over at least 200 simulations.

implementable in a physically-realizable system of building blocks interacting *via* programmable potentials. Along the way, we have outlined an approach to design catalysis from the bottom-up: by breaking up the catalytic cycle into elementary steps, we have derived necessary conditions that limit the region in the parameter space where catalysis can emerge. These conditions lead to trade-offs when simultaneously considered, as we have verified in MD simulations.

Our design rules are general and can be applied to a range of experimental systems with programmable interactions. Spherical particles with short-range specific interactions we focused on here can be easily realized with DNA-coated colloids.[4] Particle valence, which we assumed in our model, is readily available in these systems. For example, emulsion droplets functionalized with mobile DNA strands can exhibit valence by controlling the strand density.[11] Likewise, droplets can be functionalized with mobile DNA-origami constructs, where their number sets the valence.[46] Controlling the geometry of the catalyst can be achieved by patterning a surface with precisely spaced DNA patches on which catalyst particles can be deposited. Alternatively, DNA-origami constructs could also be used to fix the distance between the particles in the catalyst,[56] or the desired catalyst geometry could be 3D printed[57] and functionalized with DNA afterwards. While results in Fig. 2(A) suggest a need for strict control of particle polydispersity for catalysis to emerge in experiments, the required particle size resolution (ESI†), which depends on the interaction range r_{cutoff}, lies within the realm of current technological possibilities.[58–60]

The most favourable reaction conditions in our model require controlling the reaction between two product monomers as well as the re-binding of products to the catalyst (product inhibition). Linker-mediated interactions[44] can introduce an entropic barrier for the reformation of the substrate bond once broken, controlled by the concentration of the free floating linkers in solution. Similarly, self-protected attractions in DNA-functionalized particles could serve to minimize product inhibition.[26] Note that because our catalyst is robust, *i.e.*, the optimum ϵ_{cs}/ϵ_s remains unchanged when ϵ_s varies, the same substrate dimer and catalyst dimer could be used in experiments at a range of temperatures.

Our catalyst operates through a strain mechanism first proposed by Haldane for enzymes.[35] This is however not the only possible mechanism of catalysis. In particular, other spontaneous reactions, such as bond formation, where the barrier to overcome is entropic rather than energetic, require different mechanisms which will be interesting to investigate in future work.

Bond cleavage plays a role in essentially all reactions. Our colloidal catalyst may therefore find applications in problems of self-assembly and self-replication where bond cleavage is currently non-specific and externally driven. A catalyst provides several advantages over such protocols: it can be made specific to a particular bond, it does not require intervention and energy input, and, as we have here demonstrated, it can be implemented using the same building blocks as the rest of the system. Although minimal, our catalyst provides insights into the design principles underlying catalysis, opening the door to a control over the reactions in bio-inspired artificial systems.

Author contributions

OR and ZZ designed research; MMB performed the calculations and numerical simulations; MMB, OR and ZZ wrote the paper.

Conflicts of interest

The authors declare no conflicts of interest.

Acknowledgements

We would like to thank Jasna Brujic, Ludwik Leibler, Angus McMullen, Clément Nizak, Ben Rogers, Nicolas Bremond and Yann Sakref for insightful discussions. This work has received funding from the European Unions Horizon 2020 research and innovation program under the Marie Sklodowska-Curie grant agreement no. 754387. ZZ acknowledges funding from the city of Paris EMERGENCE(S) grant.

Notes and references

1 C. A. Mirkin, R. L. Letsinger, R. C. Mucic and J. J. Storhoff, *Nature*, 1996, **382**, 607–609.
2 A. P. Alivisatos, K. P. Johnsson, X. Peng, T. E. Wilson, C. J. Loweth, M. P. Bruchez and P. G. Schultz, *Nature*, 1996, **382**, 609–611.
3 W. B. Rogers and J. C. Crocker, *Proc. Natl. Acad. Sci. U. S. A.*, 2011, **108**, 15687–15692.
4 W. B. Rogers, W. M. Shih and V. N. Manoharan, *Nat. Rev. Mater.*, 2016, **1**, 1–14.
5 E. Elacqua, X. Zheng, C. Shillingford, M. Liu and M. Weck, *Acc. Chem. Res.*, 2017, **50**, 2756–2766.

 This journal is © The Royal Society of Chemistry 2023

Published on 15 May 2023. Downloaded by Ecole Sup de Physique et de Chimie Industrie on 5/22/2023 10:56:37 AM.

6 F. Cui, S. Marbach, J. A. Zheng, M. Holmes-Cerfon and D. J. Pine, *Nat. Commun.*, 2022, **13**, 2304.
7 L. Feng, R. Dreyfus, R. Sha, N. C. Seeman and P. M. Chaikin, *Adv. Mater.*, 2013, **25**, 2779–2783.
8 T. Hueckel, G. M. Hocky and S. Sacanna, *Nat. Rev. Mater.*, 2021, **6**, 1053–1069.
9 L. Feng, L.-L. Pontani, R. Dreyfus, P. Chaikin and J. Brujic, *Soft. Mater.*, 2013, **9**, 9816.
10 S. Angioletti-Uberti, P. Varilly, B. M. Mognetti and D. Frenkel, *Phys. Rev. Lett.*, 2014, **113**, 128303.
11 A. McMullen, S. Hilgenfeldt and J. Brujic, *Proc. Natl. Acad. Sci. U. S. A.*, 2021, **118**, e2112604118.
12 I. Chakraborty, D. J. G. Pearce, R. W. Verweij, S. C. Matysik, L. Giomi and D. J. Kraft, *ACS Nano*, 2022, **16**, 2471–2480.
13 Y. Wang, I. C. Jenkins, J. T. McGinley, T. Sinno and J. C. Crocker, *Nat. Commun.*, 2017, **8**, 14173.
14 M. He, J. P. Gales, É. Ducrot, Z. Gong, G. Yi, S. Sacanna and D. J. Pine, *Nature*, 2020, **585**, 524–529.
15 Y. Zhang, A. McMullen, L. L. Pontani, X. He, R. Sha, N. C. Seeman, J. Brujic and P. M. Chaikin, *Nat. Commun.*, 2017, **8**, 1–7.
16 Z. Zeravcic, V. N. Manoharan and M. P. Brenner, *Proc. Natl. Acad. Sci. U. S. A.*, 2014, **111**, 15918–15923.
17 J. D. Halverson and A. V. Tkachenko, *Phys. Rev. E: Stat., Nonlinear, Soft Matter Phys.*, 2013, **87**, 062310.
18 W. M. Jacobs, A. Reinhardt and D. Frenkel, *Proc. Natl. Acad. Sci. U. S. A.*, 2015, **112**, 6313–6318.
19 L. L. Ong, N. Hanikel, O. K. Yaghi, C. Grun, M. T. Strauss, P. Bron, J. Lai-Kee-Him, F. Schueder, B. Wang, P. Wang, J. Y. Kishi, C. Myhrvold, A. Zhu, R. Jungmann, G. Bellot, Y. Ke and P. Yin, *Nature*, 2017, **552**, 72–77.
20 M. Y. B. Zion, X. He, C. C. Maass, R. Sha, N. C. Seeman and P. M. Chaikin, *Science*, 2017, **358**, 633–636.
21 A. Neophytou, V. N. Manoharan and D. Chakrabarti, *ACS Nano*, 2021, **15**, 2668–2678.
22 A. McMullen, M. Muñoz-Basagoiti, Z. Zeravcic and J. Brujic, *Nature*, 2022, **610**, 502–506.
23 Y. Zhang, V. Pan, X. Li, X. Yang, H. Li, P. Wang and Y. Ke, *Small*, 2019, **15**, 1900228.
24 W. B. Rogers and V. N. Manoharan, *Science*, 2015, **347**, 639–642.
25 J. S. Oh, G.-R. Yi and D. J. Pine, *ACS Nano*, 2020, **14**, 4595–4600.
26 M. E. Leunissen, R. Dreyfus, R. Sha, T. Wang, N. C. Seeman, D. J. Pine and P. M. Chaikin, *Soft Matter*, 2009, **5**, 2422–2430.
27 Z. Zeravcic and M. P. Brenner, *Proc. Natl. Acad. Sci. U. S. A.*, 2014, **111**, 1748–1753.
28 R. Zhuo, F. Zhou, X. He, R. Sha, N. C. Seeman and P. M. Chaikin, *Proc. Natl. Acad. Sci. U. S. A.*, 2019, **116**, 1952–1957.
29 J. Kim, J. Lee, S. Hamada, S. Murata and S. Ha Park, *Nat. Nanotechnol.*, 2015, **10**, 528–533.
30 J. Grant, R. L. Jack and S. Whitelam, *J. Chem. Phys.*, 2011, **135**, 214505.
31 Z. Zeravcic, V. N. Manoharan and M. P. Brenner, *Proc. Natl. Acad. Sci. U. S. A.*, 2014, **111**, 15918–15923.
32 L. O. Hedges, R. V. Mannige and S. Whitelam, *Soft Matter*, 2014, **10**, 6404–6416.
33 F. Zhou, R. Sha, H. Ni, N. Seeman and P. Chaikin, *Proc. Natl. Acad. Sci. U. S. A.*, 2021, **118**, e2111193118.
34 R. Schulman, B. Yurke and E. Winfree, *Proc. Natl. Acad. Sci. U. S. A.*, 2012, **109**, 6405–6410.
35 J. B. S. Haldane, *Enzymes*, Longmans, Green and Company, 1930.
36 L. Pauling, *Chem. Eng. News*, 1946, **24**, 1375–1377.
37 P. Sabatier, in *La catalyse en chimie organique*, ed. C. Béranger, Paris, Liége, 1913.
38 L. S. Penrose and R. Penrose, *Nature*, 1957, **179**, 1183.
39 S. Miyashita, C. Audretsch, Z. Nagy, R. M. Füchslin and R. Pfeifer, *J. R. Soc., Interface*, 2015, **12**, 20141271.
40 D. Y. Zhang, A. J. Turberfield, B. Yurke and E. Winfree, *Science*, 2007, **318**, 1121–1125.
41 O. Rivoire, *J. Phys. Chem. B*, 2020, **124**, 807–813.
42 R. Niu, C. X. Du, E. Esposito, J. Ng, M. P. Brenner, P. L. McEuen and I. Cohen, *Proc. Natl. Acad. Sci. U. S. A.*, 2019, **116**, 24402–24407.
43 X. Wang, S. Ramírez-Hinestrosa, J. Dobnikar and D. Frenkel, *Phys. Chem. Chem. Phys.*, 2020, **22**, 10624–10633.
44 W. B. Rogers, *J. Chem. Phys.*, 2020, **153**, 124901.
45 Y. Wang, Y. Wang, D. R. Breed, V. N. Manoharan, L. Feng, A. D. Hollingsworth, M. Weck and D. J. Pine, *Nature*, 2012, **491**, 51–55.
46 Y. Zhang, X. He, R. Zhuo, R. Sha, J. Brujic, N. C. Seeman and P. M. Chaikin, *Proc. Natl. Acad. Sci. U. S. A.*, 2018, **115**, 9086–9091.
47 Y. Sakref, M. Muñoz-Basagoiti, Z. Zeravcic and O. Rivoire, 2023, in preparation.
48 L. Pauling, *Chem. Eng. News*, 1946, **24**, 1375–1377.
49 R. Wolfenden, *Mol. Cell. Biochem.*, 1974, **3**, 207–211.
50 B. E. Husic and V. S. Pande, *J. Am. Chem. Soc.*, 2018, **140**, 2386–2396.
51 J. D. Chodera and F. Noé, *Curr. Opin. Struct. Biol.*, 2014, **25**, 135–144.
52 M. Sarich, R. Banisch, C. Hartmann and C. Schütte, *Entropy*, 2013, **16**, 258–286.
53 R. D. Malmstrom, C. T. Lee, A. T. V. Wart and R. E. Amaro, *J. Chem. Theory Comput.*, 2014, **10**, 2648–2657.
54 A. Balandin, *Adv. Catal.*, 1969, **19**, 1–210.
55 M. D. Wodrich, B. Sawatlon, M. Busch and C. Corminboeuf, *Acc. Chem. Res.*, 2021, **54**, 1107–1117.
56 D. Hayakawa, T. E. Videbaek, D. M. Hall, H. Fang, C. Sigl, E. Feigl, H. Dietz, S. Fraden, M. F. Hagan, G. M. Grason and W. B. Rogers, *Proc. Natl. Acad. Sci. U. S. A.*, 2022, **119**, e2207902119.
57 R. P. Doherty, T. Varkevisser, M. Teunisse, J. Hoecht, S. Ketzetzi, S. Ouhajji and D. J. Kraft, *Soft Matter*, 2020, **16**, 10463–10469.
58 L. Shui, E. Stefan Kooij, D. Wijnperlé, A. van den Berg and J. C. T. Eijkel, *Soft Matter*, 2009, **5**, 2708–2712.
59 J. D. Forster, H. Noh, S. F. Liew, V. Saranathan, C. F. Schreck, L. Yang, J. Park, R. O. Prum, S. G. J. Mochrie, C. S. O'Hern, H. Cao and E. R. Dufresne, *Adv. Mater.*, 2010, **22**, 2939–2944.
60 N. A. Elbers, J. Jose, A. Imhof and A. V. Blaaderen, *Chem. Mater.*, 2015, **27**, 1709–1719.